Rectification of Ion Current Determined by the Nanopore Geometry: Experiments and Modelling *

Da-Ming Zhou(周大明)[1†], Yun-Sheng Deng(邓云生)[1†], Cui-Feng Ying(应翠凤)[1,2], Yue-Chuan Zhang(张月川)[1,3], Yan-Xiao Feng(冯艳晓)[1], Qi-Meng Huang(黄绮梦)[1], Li-Yuan Liang(梁丽媛)[1], De-Qiang Wang(王德强)[1**]

[1] *Chongqing Key Laboratory of Multi-scale Manufacturing Technology, Chongqing Institute of Green and Intelligent Technology, Chongqing 400714*

[2] *Key Laboratory of Weak-Light Nonlinear Photonics (Ministry of Education), School of Physics, Nankai University, Tianjin 300071*

[3] *University of Electronic Science and Technology of China, Chengdu 611731*

(Received 13 June 2016)

We provide a way to precisely control the geometry of a SiN_x nanopore by adjusting the applied electric pulse. The pore is generated by applying the current pulse across a SiN_x membrane, which is immersed in potassium chloride solution. We can generate single conical and cylindrical pores with different electric pulses. A theoretical model based on the Poisson and Nernst–Planck equations is employed to simulate the ion transport properties in the channel. In turn, we can analyze pore geometries by fitting the experimental current-voltage (I–V) curves. For the conical pores with a pore size of 0.5–2 nm in diameter, the slope angles are around $-2.5°$ to $-10°$. Moreover, the pore orifice can be enlarged slightly by additional repeating pulses. The conic pore lumen becomes close to a cylindrical channel, resulting in a symmetry I–V transport under positive and negative biases. A qualitative understanding of these effects will help us to prepare useful solid-nanopores as demanded.

PACS: 85.35.−p, 66.10.−x, 81.16.−c, 02.60.−x DOI: 10.1088/0256-307X/33/10/108501

Solid-state nanopores have emerged as one of the powerful tools for studying ion transport, especially for single molecule detection.[1–5] In principle, nanopore sensing relies on the electrophoretically driven translocation of biomolecules through nanometer-scale holes embedded in thin insulating membranes to confine, detect and characterize the properties or the activity of individual bio-molecules electrically by monitoring transient changes in ionic current. As the channel is partially blocked by the translocating molecule, each translocating molecule produces a change of the ionic current, with respect to that which flows through the fully open pore. In particular, ignoring the contact resistance between the electrodes and the external electrolyte reservoir, the current depends primarily on the carrier behaves inside the nanopore. Moreover, some ions stick on the surface of the membrane, as well as the nanopore inner surface under general conditions. The charging conditions and the geometry of the nanopore are the main factors that determine the current amplitudes at a given bias. Given this fact, the purpose of this work is to show a simple way to fabricate nanopores on a SiN_x membrane and to analyze the pore geometries according to the rectification effects of the current.

The setup is schematically presented in Fig. 1(a). The SiN_x/Si chip is purchased from NanoPore Solutions (Portugal), with a $25\times25\,\mu m^2$ window in the center. A thin free-standing SiN_x membrane, supported by a Si frame, is mounted in a liquid cell and separates two reservoirs containing an aqueous solution of 1 M KCl with 10 mM Tris, at pH=8. Ag/AgCl electrodes immersed on both sides of the membrane are connected to a Keithley 2450 source meter (TI, USA).

A single nanopore was fabricated by applying a current pulse on the electrodes. To obtain nanopores with small size, the current pulse was increased gradually from 30 nA (see Fig. 1(b) upper panel). Meanwhile, the electric potential drop across the membrane was acquired by the source meter (see Fig. 1(b) lower panel). At the beginning, resonant tunneling current I_1 happened assisted by localized states (i.e., structure defects) inside the membrane, since the membrane was too thick for direct tunneling between the two reservoirs. Accordingly, free charges could be produced by redox reactions at the surface or by field ionization of incorporated ions. More traps were subsequently generated at high electric field in the membrane as the tunneling electrons (holes) impinge on the material.[6,7] The electric field around the traps was higher than other areas, which enforces the generation of defects. Finally, the accumulation of charge traps led to a high localized conductive path and a discrete electric breakdown event. A nanopore is formed following the removal of the defects.[8–10] The conductance increases suddenly as the ions can travel

*Supported by the National Natural Science Foundation of China under Grant Nos 61471336, 51503207 and 61504146, and the Joint-Scholar of West Light Foundation of Chinese Academy of Sciences.

**Corresponding author. Email: dqwang@cigit.ac.cn

†They contributed to this work equally.

© 2016 Chinese Physical Society and IOP Publishing Ltd

through the nanopore. Following each pulse, a transmembrane conductance G measurement is carried out to estimate the nanopore size. The mean pore diameter D is approximated by using the formula $D = G/2\sigma(1+\sqrt{1+16\sigma d/\pi G})$, where σ is the bulk solution conductivity, and d is the film thickness.[11] When the diameter approaches the predetermined value, the pulse current decreases to a small value I_2. The pulse current I_3 became zero when the desired size of the nanopore was achieved. Figure 1(c) shows a cross section of the nanopore system.

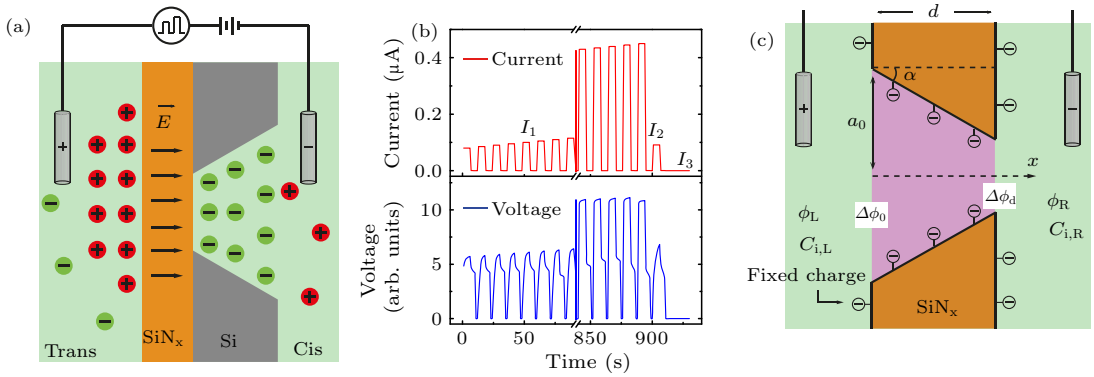

Fig. 1. Nanopore formation by dielectric breakdown. (a) A current pulse is applied across the membrane. Under the electric field, the interfaces are charged with opposite ions. Current pulse can be applied on the membrane. (b) Pulse current between the two electrodes (upper panel) and the corresponding voltage across the membrane (lower panel). (c) Schematic view of the conical nanopore with fixed charge on the surface. A negative angle α corresponds to the wide opening of the pore at the left interface.

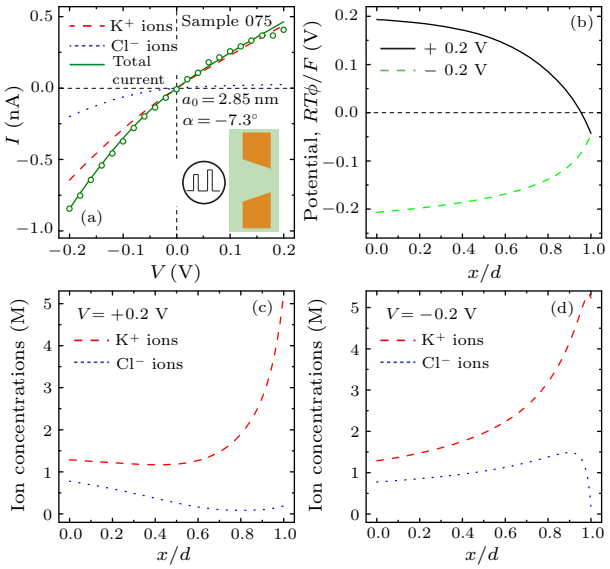

Fig. 2. Current pulses transmit from left to right (sample 075). (a) Experimentally measured (circled points) and evaluated (green solid line) currents through the channel. Red dashed and blue dotted lines are the current contributions from K^+ and Cl^- ions, respectively. The inset illustrates the pore geometry size, with a reducing radius from left to right. (b) Profiles of electric potentials in the pore lumen at the bias of $V = \pm 0.2$ V. (c, d) Concentrations of K^+ and Cl^- ions in the nanopore at the bias of $V = \pm 0.2$ V.

Firstly, a positive pulse was applied to drill the hole with a higher voltage at the trans-electrode. On the other hand, it is necessary to note that all the conductance measurements in this work are carried out with the right reservoir connected to the ground. At room temperature $T = 300$ K, the corresponding current–voltage (I–V) results (data points) through nanopore are given in Fig. 2(a). It is worth noting that there is no current in the system at zero bias. This is due to the fact that on both sides of the pore, the solutions have identical concentration, thus diffusion current does not occur accordingly. Otherwise, even at zero bias, ions will flow from the concentrated solution towards the diluted one, giving rise to a net current.[12] Significantly, the current curve exhibited rectification phenomena with higher conducting states at $V < 0$ than the one at $V > 0$. For convenience of discussion, we introduce a parameter $\gamma = |I_{+0.2\mathrm{V}}/I_{-0.2\mathrm{V}}|$ to demonstrate the asymmetry factor of the current. For instance, the present device, sample 075, has $\gamma = 0.48 < 1$.

To explain the observed phenomena qualitatively, the experimental results were fitted by classic theory simulations. In Fig. 1(c), we use a cone to model the pore shape.[13] It has symmetry of revolution around the x-axis that goes through the center part towards right side, with $x = 0$ at the left interface. The pore walls present fixed charge groups which are assumed to be homogeneously distributed on the pore surface with density σ (with its sign). The pore radius varies linearly from a_0 at the one border to a_d. The radius can be described as

$$a_x = a_0 + x\tan\alpha. \tag{1}$$

The sign of the pore slope angle α represents orientation of the nanopore. A positive (negative) α indicates the pore tip locating at the left (right) interface. The surface charge density σ and the volume concentration of fixed charges X (with its sign) are related by[14–16]

$$X = \frac{2\sigma}{aF}. \tag{2}$$

In Fig. 1(c), $c_{i,\mathrm{L}}$ and $c_{i,\mathrm{R}}$ refer to the concentration of the species i in the bulk of the bathing solution ($i = 1$ for the K^+ ion and $i = 2$ for the Cl^- ion). In our case, $c_{i,\mathrm{L}} = c_{i,\mathrm{R}} \equiv c_0 = 10^3\,\mathrm{mol{\cdot}m^{-3}}$. Here $\phi_{\mathrm{L,R}}$ are the dimensionless electric potential in units of RT/F, where R is the gas constant, T is the absolute temperature, and F is the Faraday constant. The potential drops $\Delta\phi_0 = \phi_0 - \phi_{\mathrm{L}}$ and $\Delta\phi_d = \phi_{\mathrm{R}} - \phi_d$ are, respectively, the Donnan potential differences through the left and right interfaces. This approximation is widely accepted for synthetic membranes and nanopores, which are in the micrometer thickness range. According to the results reported by Gillespie *et al.*, when the system was further scaled down to nanometers, the usual treatment of the Donnan potential also could give the correct value for electrodiffusion magnitudes despite the obtained profiles of concentration and electric potential might not be accurate.[17,18] This assumption was successfully applied on biological pores in previous studies.[12,19–21] Therefore, this assumption was acceptable on our present SiN_x system, with the channel length $d = 20\,\mathrm{nm}$.

The current consists of the diffusion contribution induced by concentration gradient, and the migration driven by the external electric field. The basic equations describing the ionic transport through the pore are the Nernst–Planck equation[14–16]

$$\boldsymbol{J}_1 = -D_1(\nabla c_1 + c_1\nabla\phi), \tag{3a}$$

$$\boldsymbol{J}_2 = -D_2(\nabla c_2 - c_2\nabla\phi), \tag{3b}$$

the Poisson equation

$$\nabla^2\phi = -\frac{F^2}{\varepsilon RT}(c_1 - c_2), \tag{4}$$

and the continuity equation

$$\nabla\cdot\boldsymbol{J}_1 = \nabla\cdot\boldsymbol{J}_2 = 0, \tag{5}$$

where $\boldsymbol{J}_{1,2}$ denote the current density of K^+ and Cl^-, respectively, $D_{1,2}$ are ion coefficients, given by $D_1 = 1.95\times10^{-9}\,\mathrm{m^2{\cdot}s^{-1}}$, $D_2 = 2.03\times10^{-9}\,\mathrm{m^2{\cdot}s^{-1}}$,[15] and ε is the electric permittivity of the solution within the pore.

For simplicity, suppose that the ionic fluxes only have an axial component along x axis. Thus

$$\boldsymbol{J}_1 \approx J_1\cdot\hat{e}_x,\ \boldsymbol{J}_2 \approx J_2\cdot\hat{e}_x. \tag{6}$$

Then Eq. (3) reads

$$J_1 = -D_1\Big(\frac{dc_1}{dx} + c_1\frac{d\phi}{dx}\Big), \tag{7a}$$

$$J_2 = -D_2\Big(\frac{dc_2}{dx} - c_2\frac{d\phi}{dx}\Big). \tag{7b}$$

The ion flows steadily in the hole, which means that the currents remain constant through an arbitrary section of the pore. Equation (5) evolves into

$$\frac{d(\pi a^2 J_1)}{dx} = \frac{d(\pi a^2 J_2)}{dx} = 0. \tag{8}$$

In addition, in the case of pores, the Poisson equation will be replaced by the electroneutrality condition[22]

$$c_1 - c_2 + X = 0. \tag{9}$$

Again, considering the Donnan equilibrium on both channel solution interfaces, the ionic concentrations and electric potential can be obtained at the pore borders $x = 0$ and d,[12,17,18]

$$c_{10} = c_0\cdot e^{-\Delta\phi_0},\ c_{1d} = c_0\cdot e^{\Delta\phi_d}, \tag{10a}$$

$$c_{20} = c_0\cdot e^{\Delta\phi_0},\ c_{2d} = c_0\cdot e^{-\Delta\phi_d}. \tag{10b}$$

Combining Eqs. (9) and (10), the ionic concentrations at the pore/external solution interfaces yield

$$c_{10} = -\frac{X_0}{2} + \Big[\Big(\frac{X_0}{2}\Big)^2 + c_0^2\Big]^{1/2}, \tag{11a}$$

$$c_{1d} = -\frac{X_d}{2} + \Big[\Big(\frac{X_d}{2}\Big)^2 + c_0^2\Big]^{1/2}, \tag{11b}$$

$$c_{20} = \frac{c_0^2}{c_{10}}, \tag{11c}$$

$$c_{2d} = \frac{c_0^2}{c_{1d}}. \tag{11d}$$

The potential at the border can be solved as

$$\phi_0 = \phi_{\mathrm{L}} - \ln\frac{c_{10}}{c_0}, \tag{12a}$$

$$\phi_d = \phi_{\mathrm{R}} - \ln\frac{c_{1d}}{c_0}. \tag{12b}$$

Substituting Eq. (7) into Eq. (8), one can obtain the second order differential equations of $c_{1,2}$ and ϕ. Taking account of the boundary values in Eqs. (11) and (12), and the constraint condition in Eq. (11) for any applied voltage $V \equiv RT(\phi_{\mathrm{L}} - \phi_{\mathrm{R}})/F$, the ion concentration and potential profiles can be solved numerically in Matlab. From the ionic fluxes, the total current passing through any arbitrary section of the nanopore takes the form of

$$I = F\pi a^2(J_1 - J_2). \tag{13}$$

In Fig. 2(a), the green solid line is the calculated results from Eq. (13). The red dashed and blue dotted curves are individual currents carried by K^+ and Cl^-, respectively. It is concluded from the experiment that the fixed charge density $\sigma = -0.07\,\mathrm{C{\cdot}m^{-2}}$, approximately 0.4 electrons per square nanometers.[23,24] The free parameters used are the pore size, $a_0 = 2.85\,\mathrm{nm}$, and $\alpha = -7.3°$. The positive pulse and pore profile are displayed in the inset of Fig. 2(a). Figures 2(b)–2(d) show the profiles of electric potential, concentrations of K^+ and Cl^- ions along the x-direction at $V = \pm0.2\,\mathrm{V}$. At the moment, let us come to the fundamental questions on the origin of the rectification

effect. While $a_0 > a_d$, the narrower part of the pore has a higher resistance, consuming most part of the electric potential (Fig. 2(b)). However, in the pore lumen, the fixed charges play a less important role on the free ion distributions. In the sequence, the ion concentrations vary drastically at the cone apex ($x = d$), while they become closer to the external concentration values in the lumen. It is worth noting that the concentration has a discontinuous jump or drop at $x = 0$ and d, which is attributed to the Donnan equilibrium assumption, as stated in Eq. (10). Furthermore, since the pore surface was negatively charged, while due to the neutrality requirement, the K^+ ion density should be higher than Cl^-. Under negative bias, the current entered the nanopore through the pore neck. An amount of K^+ ions were put forward into the pore by the external electric field, followed by the relatively number of Cl^- ions to ensure the electro neutrality. The resulting accumulation of charge carriers inside the pore lumen led to a high current. On the contrary, under positive bias, the potential difference drove the cations outside the pore, as well the Cl^- reduced accordingly. Therefore, this mechanism leads to higher average charge carrier densities in the pore under negative bias than those under positive bias, thus leading a higher current, which is in agreement with the results in Figs. 2(c) and 2(d).

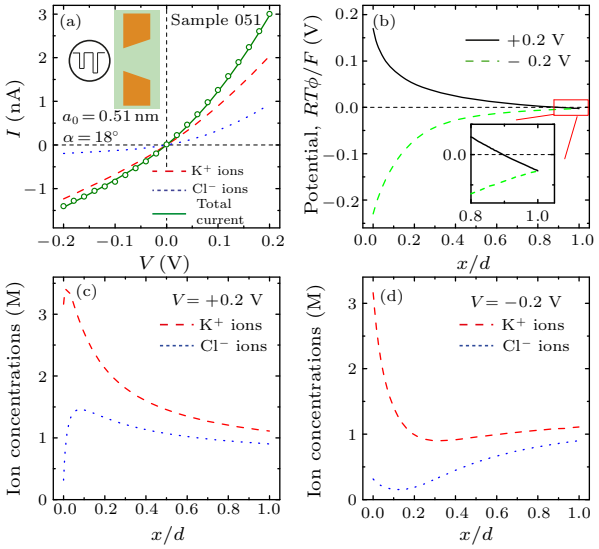

Fig. 3. Current pulses transmit from right to left (sample 051). (a) Experimentally measured (circled points) and evaluated (green solid line) currents through the channel. Red dashed and blue dotted lines are the current contributions from K^+ and Cl^- ions, respectively. (b) Profiles of electric potentials in the pore lumen at the bias of $V = \pm 0.2$ V. The potential at the end $x = d$ is enlarged in the inset panel. (c, d) Concentrations of K^+ and Cl^- ions in the nanopore at the bias of $V = \pm 0.2$ V.

To validate our model, the second group of pores is fabricated, in which the inducing current pulse emitted from the right side electrode. The corresponding conductance results of the pore are displayed in Fig. 3(a). The distinct difference from Fig. 2(a) is that the rectification parameter $\gamma = 2.1 > 1$. In the simulation, the angle α has a positive value, which is in agreement with the conclusion in the former section: the cone becomes narrower along the current pulse. This fact indicates that, in alkaline solution, the pore prefers to grow from the high potential electrode side. Assuming that trans has a high potential, the materials between the trans and one defect inside the membrane begin to dissolve under the small current. As the applied current increases slightly, more SiN_x molecules dissolve, resulting in a wider and deeper hole. This hole grows toward the cis, and the membrane is broken through lastly. Figures 3(b)–3(d) show the electric potential and ion concentrations of this sample. Both the potential and the concentrations have the prominent variations in the vicinity of $x = 0$, where the fixed charges have the more significant impact upon the ion transportation.

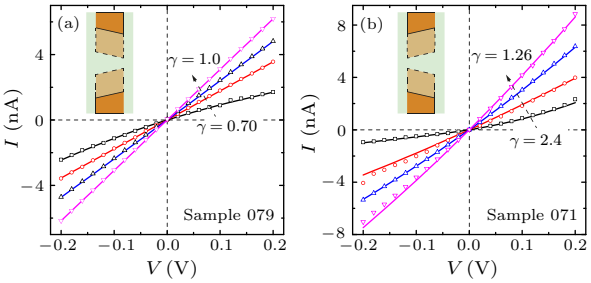

Fig. 4. Experimental I–V curves of two separate samples. Along the arrow direction, the pore is enlarged by repeating pulses, resulting in a higher current and a more symmetrical shape.

In our experiments, the reproducible results confirmed the phenomena that when the generation current pulse transmitted from trans to cis, the device had a negative α with $\gamma < 1$, while a positive α with $\gamma > 1$ when the electrodes polarity was exchanged. In addition, to study the electric breakdown mechanism, the hole can be further enlarged by repeating the pulse after the formation of the hole. From the results given in Figs. 4(a) and 4(b), it is observed that the conductance increases gradually when the hole is enlarged. We also calculate the currents for each curve, the pore radius a_0 increases, and the slope of the surface decreases. Indeed, the radius is the main factor which determines the conductance amplitude, while the rectification parameter is governed by the angle α and the surface charge density σ.[21] For sample 079, at the beginning, it has a smaller pore and stronger rectification parameter ($a_0 = 3.46$ nm, and $\gamma = 0.70$). However, the repeating pulse gives rise to a wider conic orifice, and a more symmetric conductance curve ($a_0 = 3.58$ nm, and $\gamma = 1.0$). Sample 071 exhibits the identical characteristics as 079. The enlarged hole has been schematically displayed in the two panels in Fig. 4.

In conclusion, we have presented an automatic,

simple and low-cost method to fabricate nanochannels in SiN_x membranes. In terms of the average ionic concentrations and electric potential profiles within the pore, we have explained the rectification properties of the nanopore using a continuum approach based on the Poisson–Nernst–Planck equations. Specifically, the cone orientation of the nanopores can be modulated by the polarity of the stimulus current pulse, and thus leading to the different current asymmetric factor γ. In addition, the size of these nanopores can be gradually enlarged by a repeating pulse, while the pore shape evolves from conical into cylindrical. Because single conical tracks are the elementary building blocks for nanoporous membranes, the understanding and controlling of their individual properties will be helpful for researchers to design nanofluidic devices for the application in single molecule detection and relevant applications.

We would like to thank Bin Ye and Weidong Zhang for fruitful discussions on the PNP equation solution.

References

[1] Fologea D, Ledden B, McNabb D S and Li J L 2007 *Appl. Phys. Lett.* **91** 053901
[2] Dekker C 2007 *Nat. Nanotechnol.* **2** 209
[3] Tang Z P, Lu B, Zhao Q, Wang J J, Luo K F and Yu D P 2014 *Small* **10** 4332
[4] Gilboa T and Meller A 2015 *Analyst* **140** 4733
[5] Tan S W, Gu D J, Liu H and Liu Q J 2016 *Nanotechnology* **27** 155502
[6] Feng Y, Lee K, Farhat H and Kong J 2009 *J. Appl. Phys.* **106** 104505
[7] Feng Y and Chen K 2015 *Nanotechnology* **26** 035302
[8] Habermehl S, Apodaca R T and Kaplar R J 2009 *Appl. Phys. Lett.* **94** 012905
[9] Yanagi I, Akahori R, Hatano T and Takeda K 2014 *Sci. Rep.* **4** 5000
[10] Harold K, Kyle B and Vincent T C 2014 *PLoS ONE* **9** e92880
[11] Kuan Aaron T, Lu B, Xie P, Szalay T and Golovchenko J A 2015 *Appl. Phys. Lett.* **106** 203109
[12] Queralt-Martín M, García-Giménez E, Aguilella V M, Ramírez P, Mafé S and Alcaraz A 2013 *Appl. Phys. Lett.* **103** 043707
[13] Siwy Z, Gu Y, Spohr H A, Baur D, Wolf-Reber A, Spohr R, Apel P and Korchev Y E 2002 *Europhys. Lett.* **60** 349
[14] Cervera J, Schiedt B, Neumann R, Mafé S and Ramírez P 2006 *J. Chem. Phys.* **124** 104706
[15] Ramírez P, Apel P Y, Cervera J and Mafé S 2008 *Nanotechnology* **19** 315707
[16] Nasir S, Ramírez P, Ali M, Ahmed I, Fruk L, Mafé S and Ensinger W 2013 *J. Chem. Phys.* **138** 034709
[17] Gillespie D and Eisenberg R S 2001 *Phys. Rev.* E **63** 061902
[18] Aguilella-Arzo M, García-Celma J J, Cervera J, Alcaraz A and Aguilella V M 2007 *Bioelectrochemistry* **70** 320
[19] Misakian M and Kasianowicz J J 2003 *J. Membr. Biol.* **195** 137
[20] Bhattacharya S, Muzard J, Payet L, Mathé J, Bockelmann U, Aksimentiev A and Viasnoff V 2011 *J. Phys. Chem.* C **115** 4255
[21] Payet L, Martinho M, Merstorf C, Pastoriza-Gallego M, Pelta J, Viasnoff V, Auvray L, Muthukumar M and Mathé J 2015 *Biophys. J.* **109** 1600
[22] Manzanares J A, Mafé S and Pellicer J 1992 *J. Chem. Soc. Faraday Trans.* **88** 2355
[23] Smeets R M M, Keyser U F, Krapf D, Wu M Y, Dekker N H and Dekker C 2006 *Nano Lett.* **6** 89
[24] Hoogerheide D P, Garaj S and Golovchenko J A 2009 *Phys. Rev. Lett.* **102** 256804